Structure Refinement and Magnetic Properties of Ce_2RuAl_3 and a Group-Subgroup Scheme for $Ce_5Ru_3Al_2$

Trinath Mishra, Rolf-Dieter Hoffmann, Christian Schwickert, and Rainer Pöttgen

Institut für Anorganische und Analytische Chemie, Universität Münster, Corrensstraße 30, 48149 Münster, Germany

Reprint requests to R. Pöttgen. E-mail: pottgen@uni-muenster.de

Z. Naturforsch. **2011**, *66b,* 771 – 776; received June 22, 2011

The hexagonal Laves phase Ce_2RuAl_3 ($\equiv CeRu_{0.5}Al_{1.5}$) was synthesized by high-frequence-melting of the elements in a sealed tantalum tube and subsequent annealing. The structure was refined from single-crystal X-ray diffraction data: $MgZn_2$ type, $P6_3/mmc$, $Z = 2$, $a = 565.38(9)$, $c = 888.3(1)$ pm, $wR2 = 0.0231$, 193 F^2 values and 13 parameters. The 2*a* (0.824 Ru + 0.176 Al) and 6*h* (0.956 Al + 0.044 Ru) Wyckoff positions show mixed occupancies leading to the composition $CeRu_{0.48}Al_{1.52}$ for the investigated crystal. The aluminum atoms build up Kagomé networks at $z = 1/4$ and $z = 3/4$ which are connected to a three-dimensional network by the ruthenium atoms. The cerium atoms fill cavities of coordination number 16 (3 Ru + 9 Al + 4 Ce) within the $[RuAl_3]$ network. The Ce_2RuAl_3 sample orders ferromagnetically at $T_C = 8.0(1)$ K. The cerium-rich aluminide $Ce_5Ru_3Al_2$ shows unusually short Ce–Ru distances of 253 and 260 pm for the Ce1 position as a result of intermediate cerium valence. The structural distortions are discussed on the basis of a group-subgroup scheme for $Pr_5Ru_3Al_2$ (space group $I2_13$) and the superstructure variant $Ce_5Ru_3Al_2$ (space group $R3$).

Key words: Cerium, Intermetallics, Crystal Structure, Magnetic Properties

Introduction

Unusually short Ce–Ru distances (down to 230 pm!) have recently been observed in a variety of intermetallic $Ce_xRu_yX_z$ (X = Mg, Al, Zn, Cd, In, Sn) compounds. A first overview on these materials is given in [1]. These short distances are directly related to the presence of intermediate-valent or almost tetravalent cerium, associated with strong covalent Ce–Ru bonding. Depending on the number of crystallographically independent cerium sites, different scenarios are possible. If a given structure contains only one cerium site, *e. g.* $CeRu_2Mg_5$ [2], the compound shows intermediate cerium valence. On the other hand, if two or more crystallographically independent cerium sites are available in a crystal structure, a mixed cerium valence is possible as recently observed for CeRuSn [3 – 5] and Ce_2RuZn_4 [6, 7]. The latter two compounds show a 1 : 1 ordering of trivalent and intermediate-valent cerium.

Since our last review [1], new compounds $Ce_{23}Ru_7Mg_4$ [8], $Ce_5Ru_3Al_2$ [9], $Ce_{11}Ru_2Al_6$ [10], $Ce_{16}Ru_{8.29}In_{2.71}$ [11], and $Ce_2Ru_4Mg_{17}$ [12] have been reported. They all show the same crystal chemical peculiarities and a reduced magnetic moment. The various Ce–Ru distances of these compounds are listed in Table 1. In the course of our systematic investigations of such $Ce_xRu_yX_z$ intermetallics we have obtained single crystals of the hexagonal Laves phase Ce_2RuAl_3. Preliminary powder X-ray diffraction data were reported by Schank *et al.* [13] resulting from phase analytical studies of diverse Ce-*T*-Al systems. This $MgZn_2$-type Laves phase has a quite broad homogeneity range $CeRu_xAl_{2-x}$ which approaches closely the equiatomic phase CeRuAl [1, 13]. We have obtained a sample which is close to the composition Ce_2RuAl_3 ($\equiv CeRu_{0.5}Al_{1.5}$) and allows ordering of the ruthenium and aluminum atoms on Wyckoff positions 2*a* and 6*h*. Additionally we worked out a group subgroup scheme for the structures of $Pr_5Ru_3Al_2$ and $Ce_5Ru_3Al_2$ [9] which relates the structural distortions to the short Ce–Ru distances.

Experimental

Synthesis

Starting materials for the synthesis of the Ce_2RuAl_3 ($\equiv CeRu_{0.5}Al_{1.5}$) sample were a cerium ingot (Johnson

Table 1. Ce–Ru distances (pm) of the first coordination spheres for some ternary intermetallic compounds.

Compound	Atom	Ce–Ru distances
Ce_2RuAl_3	Ce	318, 330
$Ce_5Ru_3Al_2$ [9]	Ce1	253, 260, 339, 343
	Ce2	292, 296, 304
	Ce3	295, 296, 327, 329
	Ce4	277 (3×)
$Ce_{11}Ru_2Al_6$ [10]	Ce1	323 (2×)
	Ce3	328 (2×)
	Ce4	244
	Ce5	291, 361
$Ce_{16}Ru_{8.29}In_{2.71}$ [11]	Ce1	287, 298, 304, 335
	Ce2	288 (2×), 302 (2×)
	Ce3	258 (2×), 313 (2×)
	Ce4	293 (2×), 326 (2×)
$Ce_2Ru_4Mg_{17}$ [12]	Ce	231 (2×)
$CeRu_2Mg_5$ [2]	Ce	232 (2×)
$Ce_{23}Ru_7Mg_4$ [8]	Ce1	299 (2×), 360 (2×)
	Ce2	292 (2×), 299
	Ce3	261, 275
	Ce4	351 (2×)
	Ce5	288 (2×), 302
	Ce6	339, 358
	Ce7	301 (3×)
	Ce8	287 (3×)
	Ce9	276 (2×), 380

Matthey), ruthenium powder (Degussa-Hüls) and pieces of an aluminum rod (Koch chemicals). In the first step, a piece of the cerium ingot was arc-melted [14] under argon (*ca.* 700 mbar) to a small button. The argon was purified before with molecular sieves, silica gel, and titanium sponge (900 K). The elements were then weighed in the atomic ratio 36 : 16 : 48 and arc-welded in a tantalum ampoule. The tantalum tube was placed in a water-cooled sample chamber of an induction furnace (Hüttinger Elektronik, Freiburg, Typ TIG 1.5/300) [15]. The ampoule was rapidly heated to 1600 K and kept at that temperature for 5 min, followed by an annealing period of 4 h at 1070 K. The temperature was controlled through a Sensor Therm Metis MS09 pyrometer with an accuracy of ±30 K. The sample was then quenched by switching off the power supply. Later the tantalum ampoule was sealed in a quartz tube and annealed at 1070 K for two weeks. The silvery brittle sample could easily be separated from the tantalum tube. No reaction with the container material was evident. The polycrystalline Ce_2RuAl_3 sample is stable in air over months. Single crystals exhibit metallic luster while ground powders are dark gray.

EDX data

The single crystal investigated on the diffractometer was studied by energy dispersive analyses of X-rays (EDX) using a Zeiss EVO MA10 scanning electron microscope with CeO_2, Ru and Al as standards. The experimentally observed composition was close to the ideal one and no impurity elements were observed.

X-Ray diffraction

The polycrystalline Ce_2RuAl_3 sample was characterized by a Guinier powder pattern (Cu$K_{\alpha1}$ radiation, α-quartz: a = 491.30, c = 540.46 pm as internal standard). The Guinier camera was equipped with an imaging plate unit (Fuji film, BAS-READER 1800). The hexagonal lattice parameters (Table 2) were obtained from a least-squares fit. Correct indexing was ensured by an intensity calculation [16].

Suitable single crystals were selected from the crushed Ce_2RuAl_3 sample and were investigated by Laue photographs on a Buerger camera. A data set of a high-quality crystal was collected at r. t. using a STOE IPDS-II image plate system (graphite-monochromatized MoK_α radiation; λ = 71.073 pm) in oscillation mode, and a numerical absorption correction was applied to this data set. All relevant crystallographic data are listed in Table 2.

Structure refinement

The data set showed a hexagonal lattice with high Laue symmetry, and the systematic extinctions were compatible with space group $P6_3/mmc$. The starting atomic parameters were deduced from Direct Methods with SHELXS-97 [17], and the structure was refined using SHELXL-97 [18] (full-matrix least-squares refinement on F^2) with anisotropic atomic displacement parameters for all sites. In the initial model, the Wyckoff sites 2*a* and 6*h* were refined with the scattering factors of ruthenium and aluminum, respec-

Table 2. Crystallographic data and structure refinement for $CeRu_{0.48}Al_{1.52}$.

Empirical formula	$CeRu_{0.48}Al_{1.52}$
Molar mass, g mol^{-1}	229.46
Space group; Z	$P6_3/mmc$; 2
Structure type	$MgZn_2$
Lattice parameters (Guinier powder data)	
a, pm	565.38(9)
c, pm	888.3(1)
Cell volume V, nm^3	0.2459
Crystal size, μ m^3	30 × 40 × 40
Calculated density, g cm^{-3}	6.20
Transm. ratio (max / min)	0.803 / 0.661
Radiation	MoK_α
λ, pm	71.073
Absorption coefficient, mm^{-1}	21.5
F(000), e	395
θ range, deg	4 – 32
Range in *hkl*	±8, ±8, ±13
Total reflections	2765
Independent reflections / R_{int}	193 / 0.0535
Reflections with $I \geq 2\sigma(I)$ / R_σ	166 / 0.0194
Data / parameters	193 / 13
Goodness-of-fit	1.154
$R1$ / $wR2$ for $I \geq 2\sigma(I)$	0.0140 / 0.0219
$R1$ / $wR2$ for all data	0.0228 / 0.0231
Extinction coefficient	0.0175(9)
Largest diff. peak / hole, e Å^{-3}	0.92 / −0.48

Table 3. Atomic coordinates and isotropic displacement parameters (pm^2) for $CeRu_{0.48}Al_{1.52}$. U_{eq} is defined as one third of the trace of the orthogonalized U_{ij} tensor.

Atom	W. site	x	y	z	U_{eq}
Ce	4*f*	2/3	1/3	0.05461(3)	106(1)
0.824(6) Ru + 0.176(6) Al	2*a*	0	0	0	80(2)
0.956(3) Al + 0.044(3) Ru	6*h*	0.16309(15)	2*x*	1/4	108(4)

Table 4. Interatomic distances (pm) in the structure of $CeRu_{0.48}Al_{1.52}$. All distances within the first coordination shells are listed. Standard deviations are all equal or smaller than 0.3 pm. Note that the Ru and Al sites show mixed occupancy (Table 3).

Ce:	3	Al	317.8	Al:	2	Ru	273.5
	3	Ru	330.0		2	Al	276.6
	6	Al	331.7		2	Al	288.7
	3	Ce	340.5		2	Ce	317.8
	1	Ce	347.1		4	Ce	331.7
Ru:	6	Al	273.5				
	6	Ce	330.0				

tively. The resulting equivalent isotropic displacement parameters were too high for the ruthenium and too low for the aluminum position, a clear indication for Ru/Al mixing on both sites. In the subsequent cycles we allowed for mixed occupancy on both sites, leading to the composition $CeRu_{0.48}Al_{1.52}$ for the investigated crystal. The final difference Fourier synthesis revealed no significant residual peaks (Table 2). The atomic parameters and interatomic distances are listed in Tables 3 and 4.

Further details of the crystal structure investigation may be obtained from Fachinformationszentrum Karlsruhe, 76344 Eggenstein-Leopoldshafen, Germany (fax: +49-7247-808-666; e-mail: crysdata@fiz-karlsruhe.de, http://www.fiz-informationsdienste.de/en/DB/icsd/depot_anforderung.html) on quoting the deposition number CSD-423190.

Magnetic measurements

The magnetic measurement of the Ce_2RuAl_3 sample was carried out on a Quantum Design Physical Property Measurement System (PPMS) using the VSM option. The sample was packed in kapton foil and attached to the sample holder rod for measuring the magnetic properties in the temperature range 3 – 300 K with magnetic flux densities up to 80 kOe.

Discussion

Crystal chemistry of Ce_2RuAl_3

The unit cell of the Ce_2RuAl_3 ($\equiv CeRu_{0.5}Al_{1.5}$) structure is presented in Fig. 1. We first discuss the ideal structure and will then draw back to the homogeneity range. The aluminum atoms build up Kagomé

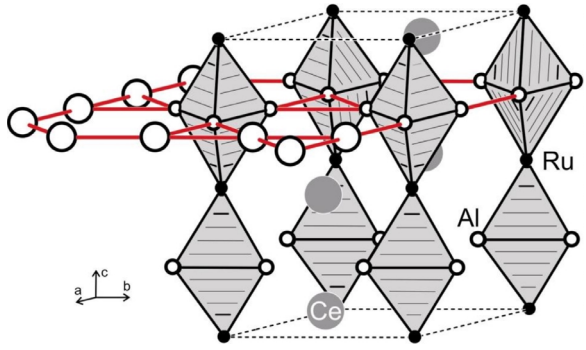

Fig. 1 (color online). The structure of the hexagonal Laves phase Ce_2RuAl_3. The rows of corner- and face-sharing $RuAl_3$ tetrahedra are emphasized. The Kagomé network of the aluminum atoms at $z = 3/4$ is drawn in red color.

networks in the *xy* plane at $z = 1/4$ and $z = 3/4$ with Al–Al distances of 277 and 289 pm, comparable to that in the structure of *fcc* aluminum (286 pm) [19]. The Al_3 triangles of these networks are coordinated to the ruthenium atoms in a sandwich-like manner. Within these $RuAl_6$ trigonal prisms the Ru–Al distances of 274 pm are significantly longer than the sum of the covalent radii of 243 pm [20], indicating weaker Ru–Al bonding character. Similar Ru–Al distances occur in the structures of the aluminides $Ce_{11}Ru_2Al_6$ (260 pm) [10], CeRuAl (267 – 278 pm) [21], and $Ce_5Ru_3Al_2$ (257 – 262 pm) [9].

The cerium atoms fill cavities of coordination number 16 (3 Ru + 9 Al + 4 Ce) within the three-dimensional $[RuAl_3]$ network. The four nearest cerium neighbors are at relatively close Ce–Ce distances of 341 and 347 pm, close to the Hill limit [22] of 340 pm for *f* electron localization.

Finally we draw back to the homogeneity range and the course of the lattice parameters within the solid solution $CeAl_{2-x}Ru_x$. Binary $CeAl_2$ [23] crystallizes with the structure of the cubic Laves phase $MgCu_2$. Upon slight ruthenium doping, the structure switches to hexagonal, $MgZn_2$ type. The end member of this solid solution is close to $x = 1$. There we observe a switch in structure type to LaNiAl-type CeRuAl [1, 13, 21]. Starting from $CeAl_{2-x}Ru_x$ samples with $x \approx 1$ (a = 550.5, c = 870.0 pm) [13] and x = 0.85 (a = 551.4, c = 871.5 pm) [1], the lattice parameters strongly increase towards x = 0.5, *i. e.* a = 565.4 and c = 888.3 pm. In principle, full ordering of the 2*a* and 6*h* sites is possible for a composition 2-1-3, however, our single crystal data of a sufficiently annealed sample still showed a

small degree of Ru/Al mixing on both sites, nevertheless resulting in the composition $CeRu_{0.48}Al_{1.52}$, close to the ideal values. Full ordering had been observed for Mg_2Cu_3Si [24, 25] and more recently also for the gallide Eu_2IrGa_3 [26]. Thus, the transition metal can take both positions in the ternary variants.

The influence of the valence electron concentration within the tetrahedral networks of the three different Laves phases was studied in detail by Johnston and Hoffmann [27] on the basis of extended Hückel band calculations. $CeRu_{0.48}Al_{1.52}$ is clearly positioned within the stability range for the hexagonal networks.

Magnetic properties of Ce_2RuAl_3

The temperature dependence of the magnetic susceptibility (χ and χ^{-1} data) of the Ce_2RuAl_3 sample measured in a field of 10 kOe is presented in Fig. 2. The inverse susceptibility shows a pronounced curvature in going to low temperatures. This deviation from Curie-Weiss behavior most likely results from a strong crystal field splitting of the $J = 5/2$ ground state. A linear fit in the temperature range 150 to 298 K results in an effective magnetic moment of 2.50(1) μ_B per Ce atom and a strongly negative Weiss constant $\theta_P = -45(1)$ K, in agreement with the theoretical value of 2.54 μ_B for a free Ce^{3+} ion. The ferromagnetic ordering observed around 8.0(1) K has been determined

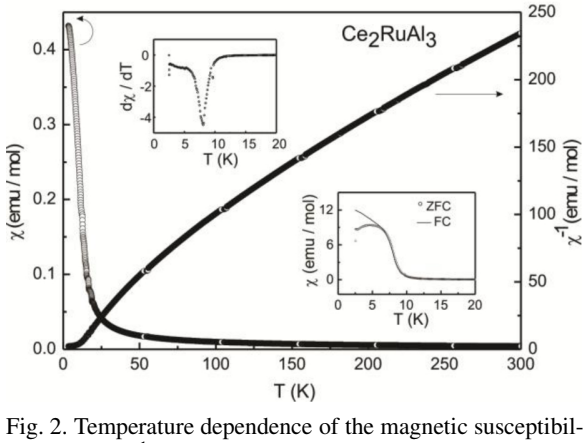

Fig. 2. Temperature dependence of the magnetic susceptibility (χ and χ^{-1} data) of Ce_2RuAl_3 measured at 10 kOe. The upper inset shows the derivative $d\chi/dT$ plot of the FC measurement, and the lower inset describes the low-temperature susceptibility (zero field cooling and field cooling modus) of Ce_2RuAl_3 at 100 Oe (kink-point measurement).

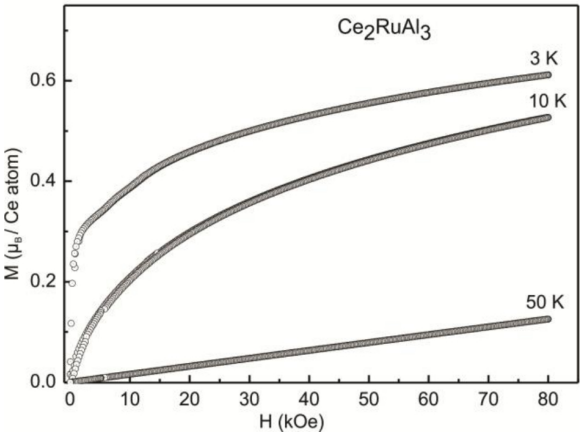

Fig. 3. Magnetization isotherms of Ce_2RuAl_3 measured at 3, 10 and 50 K.

by the derivative plot of zero field cooling and field cooling modus of Ce_2RuAl_3 at 100 Oe (kink-point measurement). This is in agreement with previous data by Schank *et al.* [13]. Ce_2RuAl_3 belongs to the rare examples of intermetallic cerium compounds with comparatively high magnetic ordering temperatures, *e. g.* CeAuGe (10 K) [28].

Fig. 3 displays the magnetization isotherms of Ce_2RuAl_3 measured at 3, 10 and 50 K with an applied external field between 0 and 80 kOe. Ce_2RuAl_3 shows a tendency for saturation at high fields. At 3 K a steep rise in M is observed, and a curvature above 10 kOe clearly indicates a canted ferromagnetic alignment in Ce_2RuAl_3. At 10 K a slight curvature is observed while at 50 K there is a linear dependence of the magnetization from the applied external field as expected for a paramagnetic material. The saturation magnetization of 0.61(1) μ_B per Ce atom at 3 K and 80 kOe is lower than the theoretical value of 2.14 μ_B per Ce atom according to $g_J \times J$. The low saturation magnetization is due to (i) crystal field splitting, and (ii) the domain structure of the Ce_2RuAl_3 sample. The single crystal data have clearly revealed small degrees of Ru/Al mixing on both sites of the tetrahedral network. Thus, the sample is expected to be composed of domains with magnetic long-range ordering with a composition very close to Ce_2RuAl_3, and domains without magnetic long-range order which slightly deviate from the ideal composition. Most cerium-based intermetallic ferromagnets with full long-range magnetic ordering show saturation magnetizations around 1 μ_B per Ce atom.

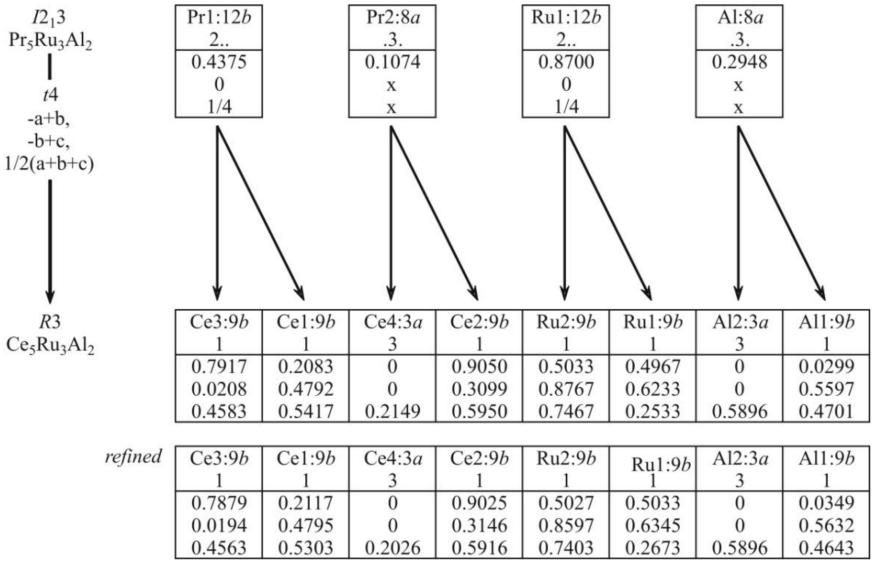

Pr1:12*b*	Pr2:8*a*	Ru1:12*b*	Al:8*a*
2..	.3.	2..	.3.
0.4375	0.1074	0.8700	0.2948
0	x	0	x
1/4	x	1/4	x

Ce3:9*b*	Ce1:9*b*	Ce4:3*a*	Ce2:9*b*	Ru2:9*b*	Ru1:9*b*	Al2:3*a*	Al1:9*b*
1	1	3	1	1	1	3	1
0.7917	0.2083	0	0.9050	0.5033	0.4967	0	0.0299
0.0208	0.4792	0	0.3099	0.8767	0.6233	0	0.5597
0.4583	0.5417	0.2149	0.5950	0.7467	0.2533	0.5896	0.4701

Ce3:9*b*	Ce1:9*b*	Ce4:3*a*	Ce2:9*b*	Ru2:9*b*	Ru1:9*b*	Al2:3*a*	Al1:9*b*
1	1	3	1	1	1	3	1
0.7879	0.2117	0	0.9025	0.5027	0.5033	0	0.0349
0.0194	0.4795	0	0.3146	0.8597	0.6345	0	0.5632
0.4563	0.5303	0.2026	0.5916	0.7403	0.2673	0.5896	0.4643

Fig. 4. Group-subgroup scheme in the Bärnighausen formalism [29 – 31] for the structures of $Pr_5Ru_3Al_2$ and $Ce_5Ru_3Al_2$ [9]. The index for the *translationengleiche* (t) symmetry reduction, the unit cell transformation, and the evolution of the atomic parameters are given. Note, various symmetry operations, transformation to the opposite absolute orientation and an origin shift t_z of 0.5896 have to be applied to meet the published data of [9].

Group-subgroup scheme for $Pr_5Ru_3Al_2$ and $Ce_5Ru_3Al_2$

The structures of the rare earth-rich aluminides $RE_5Ru_3Al_2$ (*RE* = La, Ce, Pr) [9] have recently been reported. The extremely small cell volume per formula unit (0.2466 nm^3 for $La_5Ru_3Al_2$, 0.2322 nm^3 for $Ce_5Ru_3Al_2$, and 0.2449 nm^3 for $Pr_5Ru_3Al_2$) for the cerium compound have already indicated intermediate-valent cerium. This was manifested by a significantly reduced experimental effective magnetic moment of 1.76 μ_B per Ce atom, as compared to 2.54 μ_B for a free Ce^{3+} ion.

As already stated by Murashova *et al.* [9], $Ce_5Ru_3Al_2$ (space group *R*3) adopts a rhombohedrally distorted variant of cubic $Pr_5Ru_3Al_2$ (space group $I2_13$). We now have elaborated the corresponding group-subgroup scheme (Fig. 4) in the concise and compact Bärnighausen formalism [29 – 31]. *R*3 is a *translationengleiche* subgroup of index 4 of $I2_13$. The rhombohedral distortion allows for a free c/a ratio. For $Ce_5Ru_3Al_2$ one observes a reduced value of 0.598 as compared to the ideal c/a ratio of $1/2(\sqrt{3}/\sqrt{2}) = 0.612$.

In going from the subcell to the superstructure all sites are split, leading to four cerium, two ruthenium, and two aluminum sites in the superstructure. With respect to the intermediate cerium valence the main interest lies in the cerium-ruthenium coordination. These polyhedra are presented in Fig. 5. The structural distor-

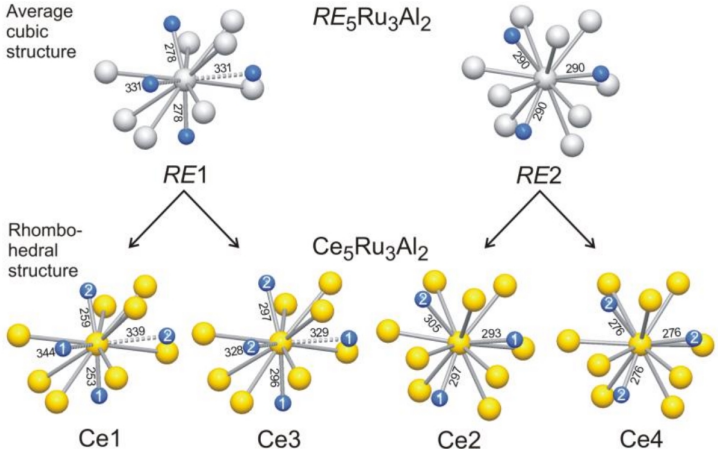

Fig. 5 (color online). Coordination polyhedra for the Ce1, Ce2, Ce3, and Ce4 atoms in $Ce_5Ru_3Al_2$ (bottom), space group *R*3 and the calculated average subcell structure $RE_5Ru_3Al_2$ (top), space group $I2_13$. Atom designations and relevant interatomic distances are indicated.

tion from cubic to rhombohedral leads to drastic differences in the cerium coordination. The largest shifts in the atomic parameters concern the ruthenium atoms. Thus, one observes 'normal' Ce–Ru distances for Ce2 and Ce3, but much shorter Ce–Ru distances for Ce1 and Ce4. The cerium atoms remain almost on the same positions. A similar ordering pattern of the ruthenium atoms has recently been observed for the superstructure of CeRuSn [3], again with the cerium atoms keeping almost their ideal positions.

Based on these group-theoretical condiderations we can conclude that the driving force of the formation of a superstructure is a bond strengthening for the ruthenium atoms which tend to fill their *d* shells. Consequently they partially oxidize the neighboring cerium atoms, leading to strong directed covalent Ce–Ru bonding. This has been manifested by electronic structure calculations for CeRuSn [3] and Ce_2RuZn_4 [7].

Acknowledgements

We thank Dipl.-Ing. U. Ch. Rodewald for the intensity data collection. This work was financially supported by the Deutsche Forschungsgemeinschaft. T. M. is indebted to the Forschungsschule *Molecules and Materials – A Common Design Principle* for a PhD fellowship.

[1] W. Hermes, S. F. Matar, R. Pöttgen, *Z. Naturforsch.* **2009**, *64b*, 901.
[2] S. Linsinger, M. Eul, U. Ch. Rodewald, R. Pöttgen, *Z. Naturforsch.* **2010**, *65b*, 1185.
[3] J. F. Riecken, W. Hermes, B. Chevalier, R.-D. Hoffmann, F. M. Schappacher, R. Pöttgen, *Z. Anorg. Allg. Chem.* **2007**, *633*, 1094.
[4] S. F. Matar, J. F. Riecken, B. Chevalier, R. Pöttgen, A. F. Al Alam, V. Eyert, *Phys. Rev. B* **2007**, *76*, 174434.
[5] J. Mydosh, A. M. Strydom, M. Baenitz, B. Chevalier, W. Hermes, B. Chevalier, *Phys. Rev. B* **2011**, *83*, 054411.
[6] R. Mishra, W. Hermes, U. Ch. Rodewald, R.-D. Hoffmann, R. Pöttgen, *Z. Anorg. Allg. Chem.* **2008**, *634*, 470.
[7] V. Eyert, E.-W. Scheidt, W. Scherer, W. Hermes, R. Pöttgen, *Phys. Rev. B* **2008**, *78*, 214420.
[8] S. Linsinger, M. Eul, W. Hermes, R.-D. Hoffmann, R. Pöttgen, *Z. Naturforsch.* **2009**, *64b*, 1345.
[9] E. V. Murashova, A. I. Tursina, N. G. Bukhanko, S. N. Nesterenko, Zh. M. Kurenbaeva, Y. D. Seropegin, H. Noël, M. Potel, T. Roisnel, D. Kaczorowski, *Mater. Res. Bull.* **2010**, *45*, 993.
[10] E. V. Murashova, A. I. Tursina, Zh. M. Kurenbaeva, H. Noël, Y. D. Seropegin, *Chem. Met. Alloys* **2010**, *3*, 101.
[11] Zh. M. Kurenbaeva, A. I. Tursina, E. V. Murashova, S. N. Nesterenko, Yu. D. Seropegin, *Russ. J. Inorg. Chem.* **2011**, *56*, 218.
[12] S. Linsinger, R.-D. Hoffmann, R. Pöttgen, unpublished results.
[13] C. Schank, F. Jährling, L. Luo, A. Grauel, C. Wassilew, R. Borth, G. Olesch, C. D. Bredl, C. Geibel, F. Steglich, *J. Alloys Compd.* **1994**, *207/208*, 329.
[14] R. Pöttgen, Th. Gulden, A. Simon, *GIT Labor-Fachzeitschrift* **1999**, *43*, 133.
[15] R. Pöttgen, A. Lang, R.-D. Hoffmann, B. Künnen, G. Kotzyba, R. Müllmann, B. D. Mosel, C. Rosenhahn, *Z. Kristallogr.* **1999**, *214*, 143.
[16] K. Yvon, W. Jeitschko, E. Parthé, *J. Appl. Crystallogr.* **1977**, *10*, 73.
[17] G. M. Sheldrick, SHELXS-97, Program for the Solution of Crystal Structures, University of Göttingen, Göttingen (Germany) **1997**. See also: G. M. Sheldrick, *Acta Crystallogr.* **1990**, *A46*, 467.
[18] G. M. Sheldrick, SHELXL-97, Program for the Refinement of Crystal Structures, University of Göttingen, Göttingen (Germany) **1997**. See also: G. M. Sheldrick, *Acta Crystallogr.* **2008**, *A64*, 112.
[19] J. Emsley, *The Elements*, Oxford University Press, Oxford **1999**.
[20] J. Donohue, *The Structures of the Elements*, Wiley, New York **1974**.
[21] A. V. Gribanov, A. I. Tursina, A. V. Grytsiv, E. V. Murashova, N. G. Bukhan'ko, P. Rogl, Y. D. Seropegin, G. Giester, *J. Alloys Compd.* **2008**, *454*, 164.
[22] H. H. Hill in *Plutonium and Other Actinides* (Ed.: W. N. Mines) Nuclear Materials Series, Vol. 17, AIME, New York, **1970**, pp. 2 – 19.
[23] H. Nowotny, *Z. Metallkd.* **1942**, *34*, 22.
[24] H. Witte, *Metallwirtschaft, Metallwissen, Metalltechnik* **1939**, *18*, 459.
[25] H. Witte, *Z. Angew. Mineral.* **1938**, *1*, 255.
[26] O. Sichevych, Yu. Prots, W. Schnelle, M. Schmidt, Yu. Grin, *Z. Kristallogr. NCS* **2006**, *221*, 263.
[27] R. L. Johnston, R. Hoffmann, *Z. Anorg. Allg. Chem.* **1992**, *616*, 105.
[28] R. Pöttgen, H. Borrmann, R. K. Kremer, *J. Magn. Magn. Mater.* **1996**, *152*, 196.
[29] H. Bärnighausen, *Commun. Math. Chem.* **1980**, *9*, 139.
[30] H. Bärnighausen, U. Müller, *Symmetriebeziehungen zwischen den Raumgruppen als Hilfsmittel zur straffen Darstellung von Strukturzusammenhängen in der Kristallchemie*, University of Karlsruhe and University/GH Kassel, **1996**.
[31] U. Müller, *Z. Anorg. Allg. Chem.* **2004**, *630*, 1519.